# Noncovalent Interactions of Metal Cations and Arenes Probed with Thallium(I) Complexes

Titel Jurca, Ilia Korobkov, Serge I. Gorelsky,* and Darrin S. Richeson*

Centre for Catalysis Research and Innovation and Department of Chemistry, University of Ottawa, Ottawa, Ontario K1N 6N5, Canada

S *Supporting Information*

ABSTRACT: The synthesis, characterization, and computational analysis of Tl(I) complexes bearing the bis(imino)-pyridine scaffold, $[\{ArN{=}CPh\}_2(NC_5H_3)]Tl^+(OTf)^-$ (Ar = 2,6-$Et_2C_6H_3$ **3**, 2,5-$^tBu_2C_6H_3$, **4**), are reported. The cations of these species showed long Tl–N and Tl–OTf distances indicating only weak or no ligand coordination. Computational analysis of the interactions between the Tl cation and the ligands (orbital populations, bond order, and energy decomposition analysis) point to only minimal covalent interactions of the cation with the ligands. The weak ligand-to-metal donation allows for additional interactions between the Tl cation and arene rings that are either intramolecular, in the case of **3**, or intermolecular. From benzene or toluene, **4** crystallizes with inverted sandwich structures having two $[\{(2,5-^tBu_2C_6H_3)N{=}CPh\}_2(NC_5H_3)]Tl^+$ cations bridged by either benzene or toluene. A density functional computational description of these Tl-arene contacts required exchange-correlation functionals with long-range exchange corrections (e.g., CAM-B3LYP or LC-PBE) and show that Tl-arene contacts are stabilized by noncovalent interactions.
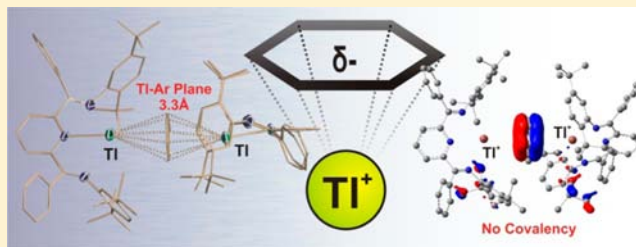
INTRODUCTION

Designing and assembling molecular architectures that promote an unusually low degree of covalency between a cation and an associated Lewis base, significantly impacts the Lewis acidity of the cation and provides insight into often overlooked noncovalent interactions. Although considered weak among structural influences, noncovalent interactions can cooperatively play a key role in fields as diverse as supramolecular/crystal engineering, molecular biology, polymer science, and broad aspects of molecular science. Inter- and intramolecular interactions involving aromatic rings are widely encountered throughout chemistry and biology and understanding the structural and energetic parameters of individual recognition modes involving these species is an active research area.[1] Metal cation-π ligand interactions involving Na^+, K^+, Mg^{2+}, and Ca^{2+} are a decidedly relevant subset of this type of interaction that are essential for the function of enzymes and ion channels.[2] Cation-π interactions are prominent across a spectrum of systems and are an important and fundamental noncovalent binding force.[3]

Recent challenges to conventional Lewis acid/base bonding description of metal–ligand interactions are provided by reports of unusual non/weakly covalent bonding in Ge(II) and In(I) complexes.[4,5] The isolation of these species and characterization, particularly by single crystal structural analysis, led to puzzling bonding issues that were addressed through computational investigations which confirmed these species exhibited only nominal classic coordination interactions. These

fundamental bonding questions have, in turn, inspired the synthesis of increasingly challenging target complexes.

Thallium with a stable monovalent state, Tl(I), and possessing filled 5d and 6s orbitals is an excellent candidate for pursuing the synthesis and analysis of noncovalently bonded compounds. The first structurally characterized Tl(I)/arene complex was reported in 1985 and thallium has since received attention for weak arene interactions.[6,3] We aimed to prepare Tl(I) compounds of the neutral pincer ligand bis(imino)-pyridine with weakly coordinating triflate anions. The planar and orthogonal disposition of the donor orbitals for this ligand should further favor unconventional noncovalent bonding with the Tl center.[7] The isolation and characterization of these species now provides unique opportunities to scrutinize weak coordination of metal centers.[8–10] The characteristic feature of such systems is that metal–ligand contacts are significantly (~0.5 Å) longer than the sum of the corresponding atomic covalent radii.
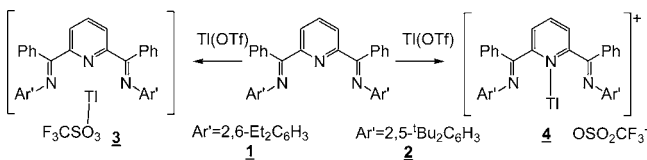
RESULTS AND DISCUSSION

Reaction of soluble $Tl(O_3SCF_3)$ with the bis(imino)pyridine scaffold, shown in Scheme 1, led to the first Tl complexes of these ligands as bright yellow species **3** (84%) and **4** (71%). Microanalyses and NMR spectroscopy confirmed the formation of the captured thallium cations as Tl-ligand complexes, $[\{ArN{=}CPh\}_2(NC_5H_3)]Tl^+$ (Ar = 2,6-$Et_2C_6H_3$,

Scheme 1

2,5-^{t}Bu$_2$C$_6$H$_3$). Compound **3** presented particular challenges with NMR characterization. In fact, only in d$_8$-toluene was the compound stable enough to obtain ^{1}H and ^{13}C NMR measurements, and both of these spectra indicate the presence of two conformers. These observations likely arise from asymmetric coordination of the (O$_3$SCF$_3$)$^-$ anion to the Tl$^+$ cation or lability of the bis(imino)pyridine ligand in the cation. Evidence for the latter proposition is provided by the fact that crystallization of **3** from diethyl ether produced a mixture of compound **3** and free ligand. Compound **4** displayed broadened NMR signals suggestive of weak association of the OTf$^-$ anion and some ligand lability. Fortunately X-ray quality crystals of both **3** and **4** could be reproducibly obtained and used to confirm the proposed identity and structural features for both of these compounds. The results of these analyses for compounds **3** and **4** are shown in Figures 1 and 2, respectively.
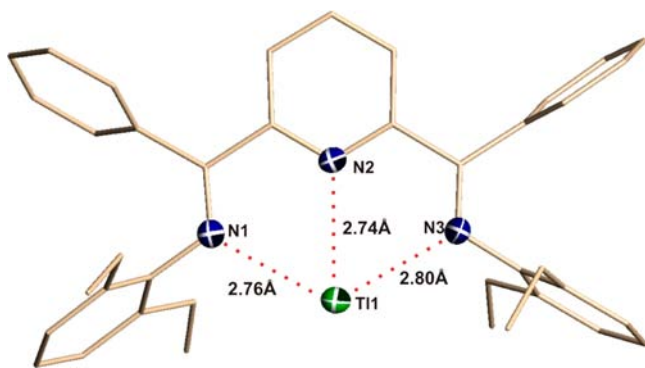

Figure 1. Structural representation of the cation in compound **3** with selected metal−ligand distances. Hydrogen atoms and the triflate counterion are omitted for clarity. Thermal ellipsoids of the ligand carbon atoms are omitted for clarity. Full structural information including a figure with thermal ellipsoids can be found in the Supporting Information.

Compound **3** displayed the expected ligand array of coplanar N atoms and with the Tl(I) residing only about 0.8 Å out of the mean plane defined by N1, N2, and N3. The metal atom is symmetrically positioned in the ligand cleft with all of the Tl−N distances longer than 2.73 Å, a value greater than the sum of the covalent radii for Tl (1.45 Å) and N (0.71 Å).[11] The shortest contact to the thallium atom is to an O atom of the triflate counterion, Tl−O1 = 2.613(2)Å.

The effects of variation on the steric load of the N−Ar′ moieties of the ligand were revealed by the distortions observed in the structure of **4** relative to compound **3**. The two N$_{imine}$ centers (N1, N3) are twisted in the same direction and out of planarity with the N$_{py}$ (N2) center. The triflate anion is considerably further away from the Tl center, and the shortest Tl−O distance is increased by >0.3 Å. The Tl center in **4**, while still positioned symmetrically with respect to the ligand, is slightly closer to the N$_{py}$ at 2.646(6)Å.
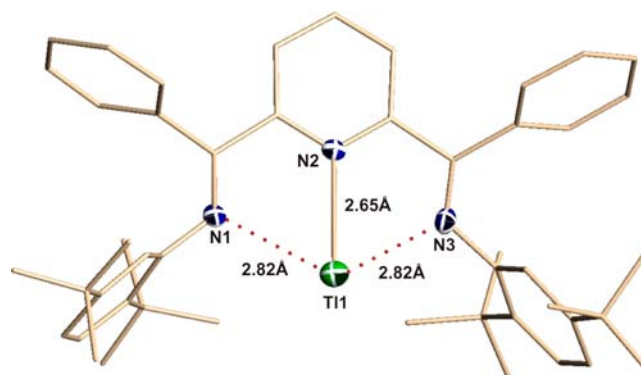

Figure 2. Structural representation of the cation in compound **4** with selected metal−ligand distances. Hydrogen atoms and the triflate counterion are omitted for clarity. Thermal ellipsoids of the ligand carbon atoms are omitted for clarity. Full structural information including a figure with thermal ellipsoids can be found in the Supporting Information.

The recently reported compound, **I**, features a monodentate bis(mesityl)pyridine coordinated Tl(I) cation complex, [Tl-(Mes$_2$py)(C$_6$H$_5$F)$_2$]$^+$ having a crystallographically characterized Tl−N distance at 2.639(6) Å which is a unique and excellent comparison for the Tl−N$_{py}$ distances of **3** and **4**.[10] Other direct comparisons for the Tl(I)-nitrogen distances in **3** and **4** are with anionic polydentate tris(pyrazolyl)borate species and bulky anionic diaryltriazenides. These compounds display shorter mean Tl−N distances of 2.63 Å and 2.59 Å, respectively.[12,13] Thallium-amido distances show, as expected, considerably shorter bond distances. For example, monomeric methyl(aryl)amido, [TlN(Me)Ar] (Ar = (2,6-Mes$_2$C$_6$H$_3$) had a Tl−N distance of 2.364(3) Å[14] and the Tl−N distance in TlN(Ar*)(SiMe$_3$) (Ar* = 2,6-{C(H)Ph$_2$}$_2$C$_6$H$_2$Me was 2.356(13) Å.[15] The gas-phase monomer TlN(SiMe$_3$)$_2$ displayed a Tl−N distance of 2.15(1) Å[16] and the mononuclear thallium(I) 1,5-diaryl-1,3,5-triazapentadienides possessed average Tl−N distances of 2.67 Å.[17]
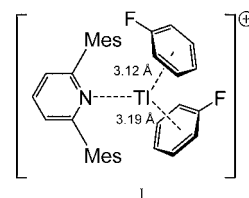
Electronic structure calculations can be used to interrogate the nature of metal−ligand interactions. Density functional theory (DFT) calculations with the B3LYP exchange-correlation (XC) functional[18,19] and the TZVP[20] basis set (the LANL2DZ basis set and effective core potential for Tl[21]) were undertaken to obtain a thorough understanding of the electronic structure of the Tl[bis(imino)pyridine]$^+$ cations in compound **3** using the X-ray structure with the optimized C−H bond distances. Within the [{ArN=CPh}$_2$(NC$_5$H$_3$)]Tl$^+$ cation of **3**, the electronic energy of the Tl−N ligand interaction was found to be −65.6 kcal/mol (−59.3 kcal/mol when the basis set superposition error (BSSE) correction[22] is applied). Only a very small component of this interaction energy is due to metal−ligand bond covalency as shown by the natural population analysis (NPA)-derived charge[23] of +0.916 au on the metal atom and the Mayer bond orders[24] of 0.12−0.14 for Tl−N interactions. The net metal−ligand bond order is 0.42,

which is considerably less than a single classical covalent bond with a bond order of 1, and distributed over three Tl−N interactions. The occupied 6s orbital of the Tl(I) does not participate in bonding to the ligand although it is mixed with many occupied ligand-based orbitals resulting in several canonical molecular orbitals with the significant Tl 6s contribution, HOMO-8 being the orbital with the largest Tl 6s contribution (Figure 3). The metal-N ligand covalent
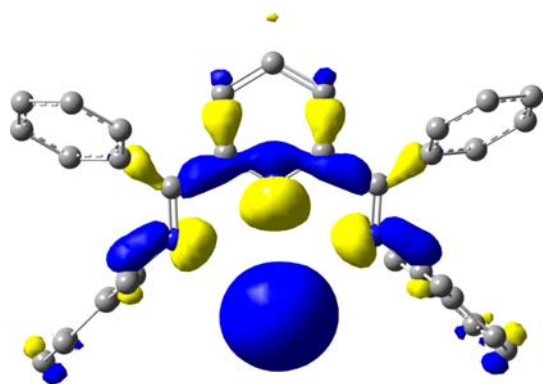

Figure 3. Isosurface plot (isovalue of 0.04 electrons Bohr^{-3}) of HOMO-8, the canonical molecular orbital of [{ArN═CPh}$_2$(NC$_5$H$_3$)]Tl$^+$ cation of **3** with the largest metal 6s contribution (30%).

bonding in **3** is less than half of that reported for the indium analogues, [{ArN═CPh}$_2$(NC$_5$H$_3$)]In$^+$.[5] A higher degree of Tl−N covalency for the diaryltriazenide complexes Tl(N$_3$Ar$_2$) is reflected by the smaller value of the NPA-derived charge of +0.698 au on the Tl atom in these complexes.[13]

Examination of the packing in the crystal structure of **3** exposed intermolecular interactions involving a Tl(I) cation-arene interaction between two of the [bis(imino)pyridine]Tl$^+$ cations (Figure 4). These intermolecular interactions place the Tl$^+$ of one species at a 3.4 Å distance positioned over the N−Ar
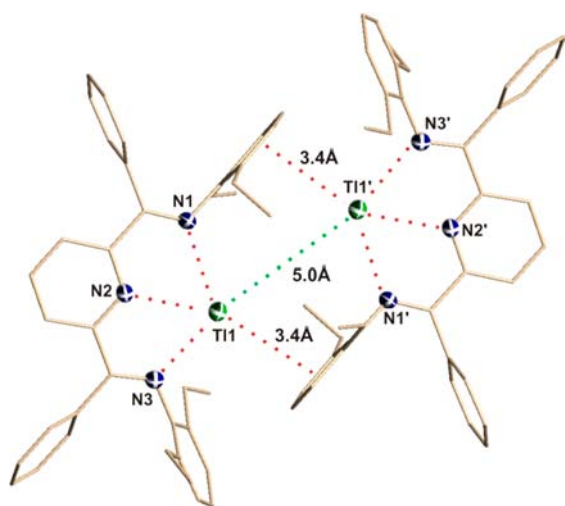

Figure 4. Structural representation of the dimer association of the cations formed through Tl-arene contacts in compound **3**. Hydrogen atoms and triflate counterions are omitted for clarity. Thermal ellipsoids of the ligand backbone carbon atoms are omitted for clarity. Full structural information including thermal parameters can be found in the Supporting Information.

group of a neighboring cation with the shortest Tl−C$_{Ar}$ contact at 3.54 Å. For comparison, the intramolecular Tl-arene interactions in monomeric methyl(aryl)amido, [TlN(Me)(2,6-Mes$_2$C$_6$H$_3$)], involved a pendant aryl moiety with a Tl-centroid distance of 3.026 Å as shown in **II**.[14a] Similar Tl(I)-arene features were observed in mononuclear thallium(I) 1,5-diaryl-1,3,5-triazapentadienides (TlN[C(C$_3$F$_7$)NAr]$_2$; Ar = mesityl, 2,6-diisopropylphenyl) (**III**), which exhibited very similar Tl-centroid distances.[17] The flanking aryl groups in the triazenide complexes Tl(N$_3$Ar$_2$) displayed intramolecular interactions with an average Tl-arene(centroid) distance of 3.15 Å. These interactions have small NPA-derived Wiberg Tl−C bond orders in the range 0.009−0.018.[13]
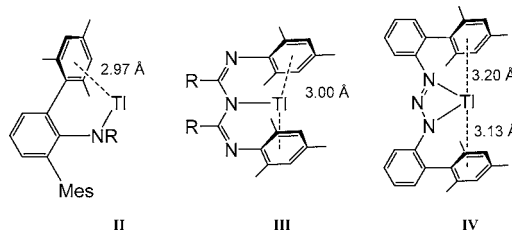
Likely because of the more bulky Ar groups, analogous intermolecular Tl-arene interactions were not observed in the X-ray structure of **4**. However, in an effort to probe the capability and nature of these cation-arene interactions, compound **4** was crystallized from benzene and toluene. Both experiments yielded unique, crystallographically characterized, inverted sandwich structures with [{(2,5-^{t}Bu$_2$C$_6$H$_3$)N═CPh}$_2$(NC$_5$H$_3$)]Tl$^+$ cations bridged by either benzene or toluene (Scheme 2).

Scheme 2
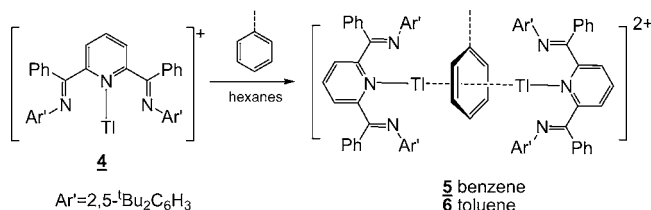
The X-ray structure for compound **5** is shown in Figure 5. The positions of the Tl and bis(imino)pyridine ligand and the Tl−N distances are similar to that observed in the parent species **4**. The shortest Tl−O(triflate) distance in **5** is 2.87 Å. Most interesting is the symmetrically bonded benzene that resides between two Tl(I) centers. The long Tl-arene centroid distance of 3.33 Å indicates a weak interaction between the metal cation and the arene. Figure 6 provides the single crystal structure for the analogous toluene complex, **6** and emphasizes the similarity to compound **5**. Consistent with the proposition that the long Tl-centroid distance in **5** is a weak interaction, an attempt to reproduce this structure by geometry optimization using the B3LYP functional without long-range corrections resulted in separation of the structure into three fragments (benzene and two Tl-bis(imino)pyridine complexes) with a large Tl−Tl separation (see Table 1). A full structure optimization of compound **5** using the B3LYP functional also gave the Tl−N, Tl−C, and Tl−Tl interatomic distances that were significantly overestimated relative to the X-ray bond distances as shown in Table 1.
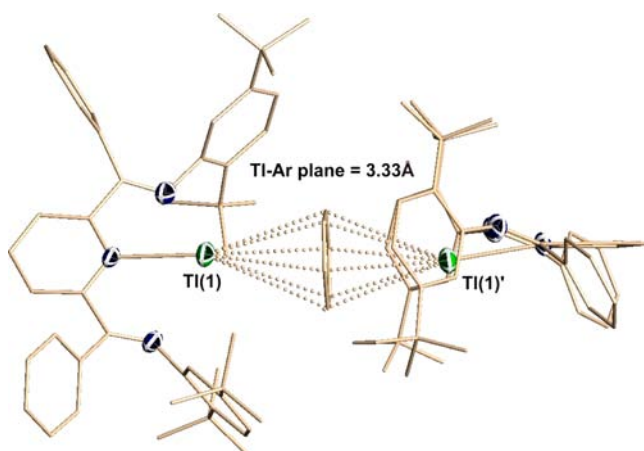
Figure 5. Structural representation of compound **5**. Hydrogen atoms and triflate anions omitted for clarity. Thermal ellipsoids of the ligand backbone carbon atoms are omitted for clarity. Full structural information including thermal parameters can be found in the Supporting Information.

Figure 6. Structural representation of compound **6**. Hydrogen atoms and triflate anions are omitted for clarity. Thermal ellipsoids of the ligand backbone carbon atoms are omitted for clarity. Full structural information including thermal parameters can be found in the Supporting Information.
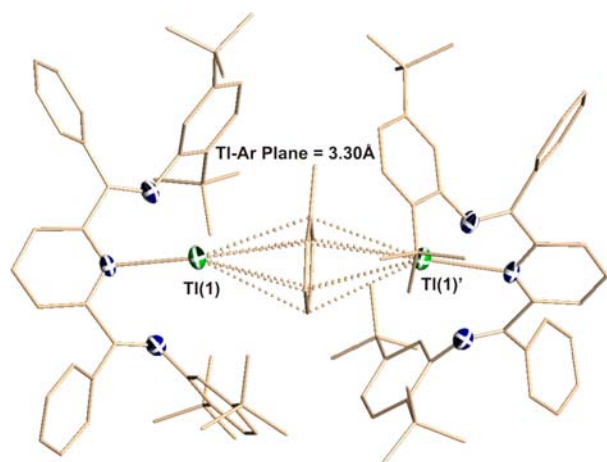
Table 1. Comparison of Selected Internuclear Distances (Å) between the Experimental (X-ray) and DFT Optimized Geometries of Compounds 3 and 5

	X-ray	LC-PBE	CAM-B3LYP	B3LYP
		Compound **3**		
Tl–N$_{imine}$	2.755(2)	2.75	2.83	2.87
	2.795(2)	2.78	2.84	2.88
Tl–N$_{pyridine}$	2.739(2)	2.75	2.82	2.84
Tl--C$_{Ar}$^{a}	3.54	3.59	3.91	4.07
Tl--Tl	5.00	4.88	5.67	6.08
		Compound **5**		
Tl–N$_{imine}$	2.809(4)	2.78	3.00	3.00
	2.827(4)	2.83	3.03	3.02
Tl–N$_{pyridine}$	2.654(3)	2.68	2.83	2.83
Tl--C$_{Ar}$^{a}	3.49	3.59	3.81	3.91
Tl--Tl	6.65	6.84	7.83	7.83

^{a}The shortest distance between the Tl atom and the carbon atom of the aryl group from the neighboring complex cation.

DFT optimization of the structure for compound **5** using the CAM-B3LYP[25] and LC-PBE[26,27] functionals with long-range exchange corrections converged to a structure that is similar to the X-ray structure (Table 1). An electronic interaction energy of −7.3 kcal/mol (−4.5 kcal/mol with the BSSE correction) between the benzene fragment and the two [{(2,5-^{t}Bu$_2$C$_6$H$_3$)-N═CPh}$_2$(NC$_5$H$_3$)]Tl$^+$(OTf)$^−$ complexes was obtained with the LC-PBE functional. The fragment molecular orbital analysis[28] of metal-arene interactions in complex **5** indicates that the occupied orbitals of the arene do not change their population upon the complex formation. Thus, this rules out a possibility of donation from the arene $π$ orbital to the empty Tl 6p orbital. The very small Mayer bond order of 0.02 between the benzene and two Tl(L)(OTf) fragments, and a charge donation of only 0.02 e$^−$ from the two metal fragments to the arene points to a very small contribution of covalent interactions to the stability of the inverted sandwich structure. Thus, contrary to the first-glance Lewis acid/base-derived covalency in such structures, the bonding between the arene and the metal fragments is dominated by noncovalent interactions.

The occurrence of structures **3**, **5**, and **6** is consistent with the propensity of Tl$^+$ to form weak noncovalent interactions with arenes. The recently reported [Tl(PhMe)$_3$]$^+$ cation is a good example of this behavior. In this structure, the metal ion shows no close contacts with anions and only Tl-arene interactions are present (average of the three Tl-arene centroid distances was 2.97 Å). DFT calculations for the [Tl(PhMe)$_3$]$^+$ cation gave a high atomic charge on the Tl atom (0.90 au), indicating very small metal-arene covalency, and the electronic interaction energy between Tl$^+$ and three toluene ligands was determined to be −17.6 kcal/mol per arene.[29] Interestingly, the bulky pyridine coordinated Tl(I) cation in **I** crystallizes associated to aromatic groups at similar interaction distances but with the aromatic moiety possessing an electron with-drawing F substituent.[10]

The B3LYP functional does not provide a balanced description for the interatomic interactions in compounds **3**, **5**, and **6** likely because of the issues with balanced treatment of long-range exchange interactions.[25,30] XC functionals with long-range exchange corrections, such as CAM-B3LYP and LC-PBE, provide a more balanced description as seen in Table 1. These functionals give bound ground states for the Tl(L)(OTf)-arene species. The calculation of electronic interaction energies between the thallium fragments and the arene is useful to investigate the magnitude of the interaction and how strongly its value depends on the XC functional employed (Table 2). Typically, three contributions are considered to be the electronic interaction energies: the electrostatic contribution, Pauli exchange, and the orbital (charge transfer) contribu-tions.[31] The small values for the bond order between the metal fragment and the arene (for example, Mayer bond order of 0.02 for Tl-arene interactions in **5**) point to a minimal contribution of charge transfer (metal−ligand covalent) interactions to the electronic interaction energy. The calculations using the three different XC functionals (B3LYP, CAM-B3LYP, and LC-PBE) provide very similar electrostatic interaction energies[32,33] regardless of the functional employed (the second column in Table 2). This shows that all three XC functionals give a very similar charge/electronic density distribution for these complexes. However, the difference is the electronic interaction energies, E_{int}, between these functionals (the third column in Table 2) highlights the fact that the repulsive Pauli exchange

Table 2. Computed Electrostatic and Electronic Interaction Energies for the Two Tl(L)(OTf) Fragments in 3 Using Three Different XC Functionals

XC functional	$E_{es}{}^{a}$ (kcal/mol)	$E_{int}{}^{b}$ (kcal/mol)
B3LYP[c]	−15.0	+3.0 (+0.9)
CAM-B3LYP[c,d]	−15.3	0.0 (−3.1)
LC-PBE[c,d]	−16.7	−5.6 (−8.9)
LC-PBE[d,e]	−17.5	−5.5 (−8.6)

[a]Electrostatic interaction energy between the fragments evaluated from NPA-derived atomic charges. [b]Electronic interaction energy between the fragments with and without the BSSE correction (the uncorrected energy values are shown in parentheses). [c]Using the X-ray structure of the compound with all C−H bond distances optimized. [d]CAM-B3LYP and LC-PBE are the functionals with long-range exchange corrections. [e]Using the fully optimized structure of the compound.

contribution to E_{int} is significantly higher (by 9.8 kcal/mol) for B3LYP than for LC-PBE. This higher Pauli exchange contribution to E_{int} leads to positive values of the electronic interaction energy (repulsive potential) for a calculation with the B3LYP functional which explains the "underbound" calculated structures with the Tl−Tl distances that are longer than the X-ray values by 1.1−1.2 Å (Table 1).

The small electronic energies for the thallium-arene interactions align with the literature in identifying the weakness of the Tl-arene bonding; however, they enhance our understanding of these interactions by identifying the key role of electrostatic and dispersion forces for these interactions. It is also possible that van der Waals/dispersion interactions, typically neglected in the standard Kohn−Sham DFT calculations[34] also contribute to stability of these Tl-arene structures. One of the approaches to account for the missing dispersion forces is an application of the empirical dispersion corrections[35] for DFT treatment with the standard XC functionals (the so-called DFT-D methods). The other approach is to use XC functionals constructed to include mid/long-range interactions or optimized in the presence of a dispersion-correction term.[36] The assessment of dispersion interactions for metal-arene structures in these thallium complexes has not been undertaken. However, since these are noncovalent contributions to bonding, their presence in these complexes will not affect the main conclusion of this work.

The features for the Tl-arene interactions are further highlighted by the fact that similar arene complexes of neighboring Au^{+} cation are rare.[37] Monovalent gold displays a similar covalent radius to Tl[+], but this cation possesses an empty 6s orbital and is a more polarizable, softer (in the hard and soft acid and base (HSAB) theory sense[38]) cation, making for a compelling comparison to thallium. In fact the first X-ray structures of gold complexes with arenes as ligands [(R₃P)Au-(arene)]⁺SbF₆⁻ (arene = toluene, p-xylene) were only recently reported.[39] These compounds were described as η¹ or η² coordinated arenes, and the shortest distances from Au^{+} to the planar arene ligands are 2.20−2.24 Å. Such structural features indicate a stronger, more directed bonding for these cation-arene species. The only other reported analogue is a related (aminocarbene)Au(toluene)⁺ cation with a B(C₆F₅)₄⁻ anion.[40] The toluene moiety was characterized as η²-coordinated to the gold center with little perturbation of the aromatic ring, implying weak coordination.

■ CONCLUSION

The reproducible isolation and crystallographic characterization of these [bis(imino)pyridine]Tl⁺ compounds provide challenges to the first impression of simple Lewis acid/base interactions and covalency between N-centered lone pairs and the metal center by presenting a unique system for examining weakly bonded species and noncovalent interactions. Importantly, these metal−ligand interactions modulate the cation-arene contacts. The structural features of these systems can be reproduced at the DFT level of theory by using exchange-correlation functionals with long-range exchange corrections. Through computational analysis and relation with reported literature complexes it becomes clear that these Tl-arene contacts are stabilized by noncovalent interactions. It is quite likely that such interactions play a key role across diverse fields of chemistry, and we continue to seek out and illustrate the importance of these noncovalent interactions.

■ EXPERIMENTAL SECTION

General Methods. Reactions were performed in a glovebox under a nitrogen atmosphere, with the exception of ligand synthesis, which was performed using standard Schlenk techniques under a flow of N₂. All solvents were sparged with nitrogen and then dried by passage through a column of activated alumina using an apparatus purchased from Anhydrous Engineering. Deuterated toluene was dried using activated molecular sieves. Thallium triflate was purchased from Strem Chemicals and used as received. All other chemicals were purchased from Aldrich and used without further purification. Compounds **1** and **2** were synthesized according to literature procedures, the crystal structure of **1** is also reported in the Supporting Information, Figure S1.[41] NMR spectra were run on a Bruker Avance 300 MHz spectrometer with C₇D₈ as solvent and internal standard. Elemental analyses for **3** and **4** were performed by Midwest Microlab LLC, Indianapolis IN.

Caution! On working with Thallium compounds, because of the well-established toxicity of thallium in the +1 oxidation state, care must be taken to prevent introduction into the body by inhalation, accidental ingestion through contaminated hands or gloves, or through the skin.[42] All thallium reagents and wastes, including contaminated solvents, were handled using multiglove and secondary containment procedures; all wastes were disposed of in accordance to government regulations.

[Tl-2,6-Bis{1-[(2,6-diethylphenyl)imino]-benzyl}pyridine]-[OSO₂CF₃] (3). TlOSO₂CF₃ powder (63 mg, 0.178 mmol) was added to a clear yellow solution of **1** (100 mg, 0.182 mmol) in 5 mL of hexanes. The reaction mixture was sealed and allowed to stir for 18 h. The solution remained opaque yellow throughout the reaction. The solution was then held at −30 °C for 24 h, and a bright yellow precipitate formed. This solution was filtered, and the precipitate was washed with 5 × 2 mL of hexanes, and allowed to dry under vacuum, resulting in the isolation of a bright yellow powder of **3** in 84% yield. Bright yellow rod-like crystals suitable for X-ray analysis were grown by evaporation from cold ether at −30 °C for several days. Crystallization yields a near 50:50 mix of bright yellow crystals corresponding to **3**, as well as pale yellow needles corresponding to free ligand **1** as a result of product decomposition. NMR experiments were conducted in C₇D₈ as the complex appears to be stable in toluene over the time period required to obtain adequate spectra. However, two distinct conformers (*i* and *ii*) of **3** are observed, with *conformer i* being predominant, the respective peaks are tentatively assigned: ¹H NMR (C₇D₈, 23 °C): δ 8.35(br s, 1H, Ar−H, *Conformer ii*), 8.25(br s, 1H, Ar−H, *Conformer i*), 7.98(br s, 4H, Ar−H, *Conformer i*), 7.73−7.10(br m, 11H_{i}, 15H_{ii}, Ar−H, *Conformers i and ii*), 6.98−6.79 (br m, 6H, Ar−H, *Conformers i and ii*), 3.04(br m, 4H, −CH₂, *Conformer i*), 2.91(br m, 4H, −CH₂, *Conformer ii*), 2.69(br m, 4H, −CH₂, *Conformer i*), 2.45(br m, 4H, −CH₂, *Conformer ii*), 1.49(br m, 12H, −CH₃, *Conformer i*), 1.25(br m, 12H, −CH₃, *Conformer ii*). ¹³C NMR (C₇D₈, 23 °C) *Conformer i:* δ 167.9 (C═N imine), 156.4(py, *m*-CH),

148.8(py, o-C=N), 139.1(py, p-CH), 135.9(Ar–CH), 132.9(Ar–CH), 131.3(Ar–CH), (Ar–CH and Ar-i-C are obscured by C_7D_8 peaks at 127–129, and 125–126 ppm), 126.6(Ar–CH), 124.8(Ar-i-C), 124.3(Ar-i-C), 26.0(–CH$_2$), 14.9(–CH$_3$). Conformer ii: δ 165.4 (C=N imine), 155.8(py, m-CH), 146.2(py, o-C=N), 138.9(py, p-CH), 135.7(Ar–CH), 132.2(Ar–CH), 129.9(Ar–CH), (Ar–CH and Ar-i-C are obscured by C_7D_8 peaks at 127–129, and 125–126 ppm), 126.1(Ar–CH), 123.9(Ar-i-C), 122.1(Ar-i-C), 25.5(–CH$_2$), 13.9-(–CH$_3$). Elemental analysis for $C_{40}H_{39}F_3TlN_3O_3S$ Calculated: C, 53.19; H, 4.35; N, 4.65 Found: C, 52.79; H, 4.63; N, 4.36.

Tl-2,6-Bis{1-[(2,5-ditertbutylphenyl)imino]-benzyl}pyridine]-[OSO$_2$CF$_3$] (4). TlOSO$_2$CF$_3$ powder (51 mg, 0.145 mmol) was added to a clear yellow solution of **2** (100 mg, 0.151 mmol) in 5 mL of hexanes. The reaction mixture was sealed and allowed to stir for 18 h. The solution remained opaque yellow throughout the reaction. The solution was then held at −30 °C for 24 h, and a bright yellow precipitate formed. This solution was filtered, and the precipitate was washed with 5 × 2 mL of hexanes, and allowed to dry under vacuum, resulting in the isolation of a bright yellow powder of **4** in 71% yield. Bright yellow rod-like crystals suitable for X-ray analysis were grown by evaporation from cold ether at −30 °C for several days. Furthermore, no evidence of decomposition of **4** is observed. ^{1}H NMR (C_6D_6, 23 °C): δ 8.26–6.73(br m, 19 H, aromatic), 1.53(br s, 18H, ^{t}Bu), 1.15(br s, 18H, ^{t}Bu). ^{13}C NMR (C_6D_6, 23 °C). δ 167.8(C=N imine), 157.7(py, o-C=N), 150.2(py, m-CH), 147.9(py, p-CH), 139.6(Ar-^{t}Bu, i-C), 138.7(Ph, o-CH), 136.2(Ar-^{t}Bu, o-CH), 131.1(Ph, i-C), 130.3(Ar-^{t}Bu, p-CH), [(Ph, p-CH) and (Ar-^{t}Bu, m-C) are obscured by C_6D_6 peak 128–130 ppm], 126.7(Ar-^{t}Bu, m-CH), 122.7(Ph, m-CH), 120.4(Ar-^{t}Bu, o-C), 35.8(Ar-^{t}Bu, CH$_3$), 34.9(Ar-^{t}Bu, CH$_3$), 31.7(Ar-^{t}Bu, CH$_3$), 31.2(Ar-^{t}Bu, CH$_3$). Elemental analysis for $C_{48}H_{55}F_3TlN_3O_3S$ Calculated: C, 56.78; H, 5.46; N, 4.14 Found: C, 55.93; H, 5.33; N, 3.93.

Preparation of Compounds 5 and 6. Single crystals of **5** and **6** suitable for X-ray crystallographic study were prepared by dissolution of **4** in the appropriate dry aromatic hydrocarbon, benzene for **5** and toluene for **6**, followed by filtration through Celite. The solution was put into a small vial which was placed within a larger vial containing dry hexanes. The concentric vials were capped tightly and cooled in a freezer at −30 °C. Crystals of **5** and **6** grew in the smaller vial during several days.

X-ray Crystallography. Data collection results for compounds **1** and **3**–**6** represent the best data sets obtained in several trials for each sample. The crystals were mounted on thin glass fibers using paraffin oil. Prior to data collection crystals were cooled to 200.15 K. Data were collected on a Bruker AXS SMART single crystal diffractometer equipped with a sealed Mo tube source (wavelength 0.71073 Å) APEX II CCD detector. Raw data collection and processing were performed with APEX II software package from BRUKER AXS.[43] Diffraction data for **1**, **5**, and **6** were collected with a sequence of 0.5° ω scans at 0, 120, and 240° in φ. Because of lower unit cell symmetry and to ensure adequate data redundancy, diffraction data for **3** and **4** were collected with a sequence of 0.5° ω scans at 0, 90, 180, and 270° in φ. Initial unit cell parameters were determined from 60 data frames with 0.3° ω scan each collected at the different sections of the Ewald sphere. Semiempirical absorption corrections based on equivalent reflections were applied.[44] Systematic absences in the diffraction data set and unit-cell parameters were consistent with triclinic $P\bar{1}$ (No. 2) for compounds **3** and **4**, monoclinic *C2/c* (No. 15) for compounds **5** and **6**, orthorhombic *Pbca* (No. 61) for compound **1**. Solutions in the centrosymmetric space groups for all compounds yielded chemically reasonable and computationally stable results of refinement. The structures were solved by direct methods, completed with difference Fourier synthesis, and refined with full-matrix least-squares procedures based on F^2.

Refinement results for the compound **4** suggested the presence of two nonmerohedrally twinned domains. Two independent orientation matrices were found using the CELL_NOW software.[45] The data set was reintegrated with two independent orientation matrices, and consecutive model refinement was performed using the HKLF5 reflection data file. Twinning domain ratio coefficient (BASF) was

refined to 0.3039. On the final refinement stage thermal motion parameters for the *t*-Bu fragments based at C(30) and C(44) suggested a rotational disorder not related to the symmetry elements. Disorder was successfully modeled; however, the set of geometrical (SADI) and thermal motion (SIMU, DELU) restraints were applied to achieve acceptable fragment geometries and thermal motion values. Disordered fragment occupancies were refined with satisfactory results at 50%: 50% for both *t*-Bu fragments.

During the final refinement of the structure of **3** the thermal parameters of the carbon atom C(29) for the Et moiety suggested positional disorder not related to symmetry elements. Position of C(29) was split in two occupational factors and were successfully refined to 70%: 30% ratio. Initial solution suggested the presence of one cocrystallized diethyl ether solvent molecule, partially occupied and disordered over two symmetry related position by an inversion center. Without introducing an excessive amount of constraints all attempts to achieve satisfactory solvent molecules geometry and thermal parameters values were unsuccessful. To conserve acceptable data to parameters ratio, the original reflection file for **3** was treated with the SQUEEZE routine of PLATON[46] with a refined void space per cell equal to 235.7 Å^3 and an electron count per cell equal to 22 electrons. These results were consistent with the presence of one-half diethyl ether molecule per cell. Final model refinement were performed against SQUEEZE alternated reflection file, nevertheless the elemental cell composition was altered to account for the presence of omitted solvent molecules.

Close examination of the thermal parameters for the coordinated toluene molecules in the structure of **6** suggested rotational disorder of the molecule with two positions related by an inversion center. Occupational factors were successfully refined to 50%: 50% ratio and set of geometry restraints (AFIX 66) and thermal parameters constraints (SIMU, DELU) were used to achieve satisfactory refinement results. Initial solution suggested the presence of two cocrystallized partially occupied toluene solvent molecules. Both solvent molecules were disordered over two symmetry related positions by an inversion center. Without introducing an excessive amount of constraints all attempts to achieve satisfactory molecular geometry and atomic thermal parameters values were unsuccessful. To conserve acceptable data to parameters ratio original reflection file for **6** was treated with the SQUEEZE routine of PLATON[42] with a refined void space per cell equal to 3624.4 Å^3 and an electron count per cell equal to 402 electrons. These results were consistent with the presence of eight toluene molecules per cell. Final model refinements were performed against SQUEEZE alternated reflection file; nevertheless the elemental cell composition was altered to account for the presence of omitted solvent molecules.

On the final refinement stages for the structure of **5** it was noticed that the thermal parameters for several structural fragments suggest the presence of disorder. Rotational disorder not related to symmetry elements was introduced for the *t*-Bu moiety based at C(30). Occupational factors for this fragment were successfully refined to 50%: 50%. A set of geometry constraints (SADI) was introduced to ensure acceptable molecular geometry for this fragment. From the thermal motion parameters it was established that both coordinated and noncoordinated benzene molecules are disordered by an inversion center. Occupational factors for coordinated benzene molecule were successfully refined to 50%: 50% ratio, and a set of geometry restraints (AFIX 66) was used to achieve satisfactory molecular geometry. Noncoordinated benzene molecule appeared to be only partially occupied, therefore occupational factors for this fragment were refined only to 25%: 25% value. Similarly to the former case, a set of geometry restraints (AFIX 66) together with a set of thermal parameters restraints were used to achieve adequate refinement results.

For all the compounds all hydrogen atoms' positions were calculated based on the geometry of the related non-hydrogen atoms. All hydrogen atoms were treated as idealized contributions during the refinement. All scattering factors are contained in several versions of the SHELXTL program library, with the latest version used being v.6.12[47]

■ COMPUTATIONAL DETAILS

DFT calculations have been performed using the Gaussian 09 package.[48] The structures of all species were optimized using the B3LYP,[18,19] CAM-B3LYP,[25] and LC[30]-PBEPBE[26,27] exchange-correlation functionals with the mixed basis set (the LANL2DZ basis set and effective-core potential for Tl[21] and the all-electron TZVP basis set[20] for all other elements) unless indicated otherwise. Tight SCF convergence criteria (10^{-8} a.u.) were used for all calculations. Wave function stability calculations were performed to confirm that the calculated wave functions corresponded to the electronic ground state. Harmonic frequency calculations with the analytic evaluation of force gradients were used to determine the nature of the stationary points.

The analysis of the molecular orbital (MO) compositions in terms of occupied and unoccupied orbitals of the fragment species (HOFOs and LUFOs, respectively) was performed, and Mayer bond orders[24] were calculated using the AOMix program.[49,50] Atomic charges were evaluated by using the natural population analysis (NPA).[23]

The basis set superposition errors (BSSE) for the electronic interaction energies were evaluated using the counterpoise method.[22]

The electrostatic interaction energies between fragments were evaluation using the point-charge approximation:[32,33]

$$E_{es} = \sum_{a \in \text{fragm.1}} \sum_{b \in \text{fragm.2}} \frac{q_a^{\text{NPA}} q_b^{\text{NPA}}}{r_{ab}} \quad \text{(in atomic units)}$$

where q^{NPA} are NPA-derived atomic charges and r_{ab} are the corresponding internuclear distances in the complex.

■ ASSOCIATED CONTENT

Ⓢ Supporting Information

Full structural information on compounds **1** and **3**−**6** as cif files. Thermal ellipsoid plots of compounds **1** and **3**−**6**. Cartesian coordinates of all the optimized geometries. This material is available free of charge via the Internet at http://pubs.acs.org.

■ AUTHOR INFORMATION

Corresponding Author

*E-mail: sgorelsk@uottawa.ca (S.I.G.), darrin@uottawa.ca (R.S.R.).

Author Contributions

The manuscript was written through contributions of all authors. All authors have given approval to the final version of the manuscript.

Notes

The authors declare no competing financial interest.

■ ACKNOWLEDGMENTS

■ REFERENCES

(1) (a) Salonen, L. M.; Ellermann, M.; Diederich, F. *Angew. Chem., Int. Ed.* **2011**, *50*, 4808. (b) Meyer, E. A.; Castellano, R. K.; Diederich, F. *Angew. Chem., Int. Ed.* **2003**, *42*, 1210.

(2) For selected examples and reviews see: (a) Gokel, G. W.; Barbour, L. J.; Ferdani, R.; Hu, J. *Acc. Chem. Res.* **2002**, *35*, 878. (b) Ma, J. C.; Dougherty, D. A. *Chem. Rev.* **1997**, *97*, 1303. (c) Kim, K. S.; Tarakeshwar, P.; Lee, J. Y. *Chem. Rev.* **2000**, *100*, 4145. (d) Abrahams, B. F.; FitzGerald, N. J.; Hudson, T. A.; Robson, R.; Waters, T. *Angew. Chem., Int. Ed.* **2009**, *48*, 3129.

(3) Coordination of neutral aromatic species to post-transition metals is reviewed in: Schmidbaur, H.; Schier, A. *Organometallics* **2008**, *27*, 2361.

(4) Rupar, P. A.; Staroverov, V. N.; Baines, K. M. *Science* **2008**, *322*, 1360.

(5) (a) Jurca, T.; Lummis, J.; Burchell, T. J.; Gorelsky, S. I.; Richeson, D. S. *J. Am. Chem. Soc.* **2009**, *131*, 4608. (b) Jurca, T.; Korobkov, I.; Yap, G. P. A.; Gorelsky, S. I.; Richeson, D. S. *Inorg. Chem.* **2010**, *49*, 10635.

(6) Schmidbaur, H.; Bublak, W.; Riede, J.; Müller, G. *Angew. Chem., Int. Ed. Engl.* **1985**, *24*, 414.

(7) For application of bis(imino)pyridine to unconventional main group chemistry see: Martin, C. D.; Le, C. M.; Ragogna, P. J. *J. Am. Chem. Soc.* **2009**, *131*, 15126.

(8) Examples of Tl(III) adducts of neutral pincer ligands: Walton, R. A. *Inorg. Chem.* **1968**, *7* (4), 640. Walton, R. A. *J. Inorg. Nucl. Chem.* **1970**, *32*, 2875.

(9) For an example of a Tl(III) coordinated by a bis(imino)pyridine-based macrocycle see: Kawasaki, Y.; Okuda, N. *Chem. Lett.* **1982**, 1161.

(10) While this manuscript was in the final stage of the preparation Aldridge and co-workers reported an unusual bulky pyridine coordinated Tl(I) cation [Tl(Mes$_2$py)]$^+$ that exhibits weak M(I)-arene (M = In and Tl) interactions. Mansaray, H. B.; Tang, C. Y.; Vidovic, D.; Thompson, A. L.; Aldridge, S. *Inorg. Chem.* **2012**, *51*, 13017.

(11) Cordero, B.; Gómez, V.; Platero-Prats, A. E.; Revés, M.; Echeverría, J.; Cremades, E.; Barragán, F.; Alvarez, S. *Dalton Trans.* **2008**, 2832.

(12) Dias, H. V. R. In *Comprehensive Coordination Chemistry II*; Elsevier Pergamon: Amsterdam, The Netherlands, 2004; Vol. 3, pp 383−463.

(13) Lee, H. S.; Hauber, S.-O.; Vinduš, D.; Niemeyer, M. *Inorg. Chem.* **2008**, *47*, 4401.

(14) (a) Wright, R. J.; Brynda, M.; Power, P. P. *Inorg. Chem.* **2005**, *44*, 3368. (b) Fox, A. R.; Wright, R. J.; Rivard, E.; Power, P. P. *Angew. Chem., Int. Ed.* **2005**, *44*, 7729.

(15) Dange, D.; Li, J.; Schenk, C.; Schnöckel, H.; Jones, C. *Inorg. Chem.* **2012**, *51*, 13050.

(16) Klinkhammer, K. W.; Henkel, S. *J. Organomet. Chem.* **1994**, *480*, 167.

(17) Dias, H. V. R.; Singh, S.; Cundari, T. R. *Angew. Chem., Int. Ed.* **2005**, *44*, 4907.

(18) Becke, A. D. *J. Chem. Phys.* **1993**, *98*, 5648.

(19) Lee, C.; Yang, W.; Parr, R. G. *Phys. Rev.* **1988**, *B37*, 785.

(20) Schafer, A.; Huber, C.; Ahlrichs, R. *J. Chem. Phys.* **1994**, *100*, 5829.

(21) Wadt, W. R.; Hay, P. J. *J. Chem. Phys.* **1985**, *82*, 284.

(22) (a) Boys, S. F.; Bernardi, F. *Mol. Phys.* **1970**, *19*, 553. (b) Simon, S.; Duran, M.; Dannenberg, J. J. *J. Chem. Phys.* **1996**, *105*, 11024.

(23) Reed, A. E.; Weinstock, R. B.; Weinhold, F. *J. Chem. Phys.* **1985**, *83*, 735.

(24) Mayer, I. *Int. J. Quantum Chem.* **1986**, *29*, 73.

(25) Yanai, T.; Tew, D.; Handy, N. *Chem. Phys. Lett.* **2004**, *393*, 51.

(26) Perdew, J. P.; Burke, K.; Ernzerhof, M. *Phys. Rev. Lett.* **1996**, *77*, 3865.

(27) Perdew, J. P.; Burke, K.; Ernzerhof, M. *Phys. Rev. Lett.* **1997**, *78*, 1396.

(28) Gorelsky, S. I.; Ghosh, S.; Solomon, E. I. *J. Am. Chem. Soc.* **2006**, *128*, 278.

(29) (a) Sarazin, Y.; Hughes, D. L.; Kaltsoyannis, N.; Wright, J. A.; Bochmann, M. *J. Am. Chem. Soc.* **2007**, *129*, 881. (b) Sarazin, Y.; Kaltsoyannis, N.; Wright, J. A.; Bochmann, M. *Organometallics* **2007**, *26*, 1811.

(30) Iikura, H.; Tsuneda, T.; Yanai, T.; Hirao, K. *J. Chem. Phys.* **2001**, *115*, 3540.

(31) (a) Kitaura, K.; Morokuma, K. *Int. J. Quantum Chem.* **1976**, *10*, 325. (b) Ziegler, T.; Rauk, A. *Theor. Chim. Acta* **1977**, *46*, 1.

(32) Gorelsky, S. I.; Basumallick, L.; Vura-Weis, J.; Sarangi, R.; Hedman, B.; Hodgson, K. O.; Fujisawa, K.; Solomon, E. I. *Inorg. Chem.* **2005**, *44*, 4947.

(33) Garon, C. N.; Gorelsky, S. I.; Sigouin, O.; Woo, T. K.; Fontaine, F. G. *Inorg. Chem.* **2009**, *48*, 1699.

(34) Grimme, S. *Comput. Mol. Sci.* **2011**, *1*, 211.

(35) (a) Grimme, S. *J. Comput. Chem.* **2004**, *25*, 1463. (b) Grimme, S. *J. Comput. Chem.* **2006**, *27*, 1787. (c) Antony, J.; Grimme, S. *Phys. Chem. Chem. Phys.* **2006**, *8*, 5287. (d) Grimme, S.; Antony, J.; Ehrlich, S.; Krieg, H. *J. Chem. Phys.* **2010**, *132*, 154104. (e) Grimme, S.; Ehrlich, S.; Goerigk, L. *J. Comput. Chem.* **2011**, *32*, 1456.

(36) Burns, L. A.; Vázquez-Mayagoitia, Á.; Sumpter, B. G.; Sherrill, C. D. *J. Chem. Phys.* **2011**, *134*, 084107.

(37) Schmidbaur, H.; Schier, A. *Organometallics* **2010**, *29*, 2.

(38) Parr, R. G.; Pearson, R. G. *J. Am. Chem. Soc.* **1983**, *105*, 7512.

(39) (a) Herrero-Gómez, E.; Nieto-Oberhuber, C.; López, S.; BenetBuchholz, J.; Echavarren, A. M. *Angew. Chem., Int. Ed.* **2006**, *45*, 5455. (b) Pérez-Galán, P.; Delpont, N.; Herrero-Gómez, E.; Maseras, F.; Echavarren, A. M. *Chem.—Eur. J.* **2010**, *16*, 5324.

(40) Lavallo, V.; Frey, G. D.; Kousar, S.; Donnadieu, B.; Bertrand, G. *Proc. Natl. Acad. Sci. U.S.A.* **2007**, *104*, 13569.

(41) Jurca, T.; Dawson, K.; Mallov, I.; Burchell, T.; Yap, G. P. A.; Richeson, D. S. *Dalton Trans.* **2010**, *39*, 1266.

(42) Galvan-Arzate, S.; Santamaria, A. *Toxicol. Lett.* **1998**, *99*, 1.

(43) *APEX Software Suite*, v.2010; Bruker AXS: Madison, WI, 2005.

(44) Blessing, R. *Acta Crystallogr.* **1995**, *A51*, 33.

(45) Sheldrick, G. *Cell_Now*; Bruker-AXS Inc.: Madison, WI, 2004.

(46) Spek, A. L. *Acta Crystallogr.* **1990**, *A46*, C-34.

(47) Sheldrick, G. M. *Acta Crystallogr.* **2008**, *A64*, 112.

(48) Frisch, M. J.; Trucks, G. W.; Schlegel, H. B.; Scuseria, G. E.; Robb, M. A.; Cheeseman, J. R.; Scalmani, G.; Barone, V.; Mennucci, B.; Petersson, G. A.; Nakatsuji, H.; Caricato, M.; Li, X.; Hratchian, H. P.; Izmaylov, A. F.; Bloino, J.; Zheng, G.; Sonnenberg, J. L.; Hada, M.; Ehara, M.; Toyota, K.; Fukuda, R.; Hasegawa, J.; Ishida, M.; Nakajima, T.; Honda, Y.; Kitao, O.; Nakai, H.; Vreven, T.; Montgomery, Jr., J. A.; Peralta, J. E.; Ogliaro, F.; Bearpark, M.; Heyd, J. J.; Brothers, E.; Kudin, K. N.; Staroverov, V. N.; Kobayashi, R.; Normand, J.; Raghavachari, K.; Rendell, A.; Burant, J. C.; Iyengar, S. S.; Tomasi, J.; Cossi, M.; Rega, N.; Millam, N. J.; Klene, M.; Knox, J. E.; Cross, J. B.; Bakken, V.; Adamo, C.; Jaramillo, J.; Gomperts, R.; Stratmann, R. E.; Yazyev, O.; Austin, A. J.; Cammi, R.; Pomelli, C.; Ochterski, J. W.; Martin, R. L.; Morokuma, K.; Zakrzewski, V. G.; Voth, G. A.; Salvador, P.; Dannenberg, J. J.; Dapprich, S.; Daniels, A. D.; Farkas, Ö.; Foresman, J. B.; Ortiz, J. V.; Cioslowski, J.; Fox, D. J. *Gaussian 09*, Revision A.02; Gaussian, Inc.: Wallingford, CT, 2009.

(49) Gorelsky, S. I. *AOMix software for molecular orbital analysis*, Version 6.8; University of Ottawa: Ottawa, Canada, 2013.

(50) Gorelsky, S. I.; Lever, A. B. P. *J. Organomet. Chem.* **2001**, *635*, 187.

5756

dx.doi.org/10.1021/ic302552v | *Inorg. Chem.* 2013, 52, 5749−5756